Eur. Phys. J. Appl. Phys. (2012) 59: 20403
DOI: 10.1051/epjap/2012120250

THE EUROPEAN PHYSICAL JOURNAL
APPLIED PHYSICS

Regular Article

Higher water splitting hydrogen generation rate for single crystalline anatase phase of TiO_2 nanotube arrays

C.W. Lai and S. Sreekantan[a]

School of Materials and Mineral Resources Engineering, Universiti Sains Malaysia, Engineering Campus, 14300 Nibong Tebal, Seberang Perai Selatan, Pulau Pinang, Malaysia

Received: 25 June 2012 / Received in final form: 2 August 2012 / Accepted: 3 August 2012
Published online: 3 September 2012 –

Abstract. This paper presents a detailed investigation on the effect of heat-treatment process on the highly ordered titanium dioxide (TiO_2) nanotube arrays in connection with the photoelectrochemical (PEC) response and hydrogen evolution rate. TiO_2 nanotube arrays have been systematically heat-treated to control the transformation of as-anodized TiO_2 amorphous structure to crystalline anatase and rutile phases. In this study, single crystalline TiO_2 anatase phase exhibited a higher PEC response and hydrogen evolution rate at 400 °C heat treatment. The photocurrent density increase was mainly attributed to the effective transport of photo-induced electrons within the single crystal anatase phase. However, polycrystalline anatase and rutile phases showed the fluctuation in lower photocurrent density upon heat treatment above 500 °C. The mobility of photo-induced electrons was obviously hindered due to the recombination losses in defect sites between the anatase and rutile phase.

1 Introduction

Nowadays, development of renewable, sustainable and green energy resources, as well as the protection of the environment by reducing the greenhouse gases, are two of the largest challenges for the human civilization [1–3]. In these aspects, hydrogen has been established as a potential future energy and possibly the best substitute for fossil fuel, such as petroleum, coal and natural gas [3–6]. The novel feature of hydrogen is that it can be produced from water using solar energy, which is an ideal fuel in the future-based pollution-free hydrogen economy. Both the energy (solar light) and reactive media (water) are readily available and are renewable [5–9]. However, in order to make the hydrogen as a commercial source of energy, it must be produced and made available at low cost without creating any misbalance in global ecology. Out of the various possible routes, PEC water splitting process is one of the most attractive methods to produce hydrogen which has high potential in hydrogen economy [7,9–13].

The PEC water splitting system involves harvesting solar energy with electrolysis of water, in which, it will split the water molecules into hydrogen gas and oxygen gas [10–14]. Over the past few years, highly ordered TiO_2 nanotube arrays have been attracting much attention and have appeared as the leading candidate in the PEC water splitting system [10,12,15–20]. Indeed, TiO_2 is an excellent corrosion-resistant material with great capacity for oxidation, non-toxicity, long-term stability and good photocatalytic property [15–20]. Besides, self-organized nanotubular architecture of TiO_2 provides a higher surface area for photocatalytic reaction to generate the charge carriers and possesses better charge transfer properties under illumination [16–22]. It is well known that anodization synthesis is the most feasible technique to produce well-aligned TiO_2 nanotube arrays as compared to other synthesis techniques, such as hydrothermal synthesis, template synthesis and sol-gel synthesis [7–12,15–22]. The main reason is attributed to its ability to produce the self-organized and highly ordered nanotube arrays with an almost perfect vertical alignment easily, in which TiO_2 grains are stretched in the tube growth direction. Thus, vertical transportation of photo-induced electrons could be enhanced and improve the PEC water splitting performance due to minimizing the recombination losses at grain boundaries [15–18,20–24].

It is a well-known fact that the properties of TiO_2 strongly depend on its crystallinity [25,26]. TiO_2 has three main crystal structures: anatase, rutile and brookite, where anatase and rutile phases have tetragonal lattice and brookite phase has orthorhombic lattice [25–29]. The structure of TiO_2 could be described in terms of chains of TiO_6 octahedral that are more distorted and exhibit different physical and chemical behaviors [27,29]. The most extensively studied is the anatase and rutile phase, whereas brookite is the least studied of TiO_2 phase [26–28]. The reasons for the lack of studies on the brookite phase could be attributed to the difficulty in

[a] e-mail: srimala@eng.usm.my

Table 1. Physical and structural properties of anatase and rutile structure of bulk TiO_2 [27,29,30].

Property	Rutile		Anatase	
Size for stable phase	>35 nm		<11 nm	
Crystal structure	(1 1 0) – Thermally stable – Bridging O_2 connects to two TiO_2 and alternating with this is a parallel phase	(0 0 1) – Thermally less, stable and restructuring >475 °C – Equatorial type double bridging O_2 alternate with single row exposed TiO_2	(1 0 1) – Corrugated – Alternating rows of five coordinate Ti atom and bridging O_2, grow at corrugation's edges	(0 0 1) – Flat – Undergo (1 × 4) reconstruction – Hydrothermally rod-like anatase
Band gap energy	3.0 eV		3.2 eV	
Specific gravity	3.9		4.0	
Light absorption	$\lambda < 385$ nm		$\lambda < 415$ nm	
Mohr's hardness	5.5		6.5–7	

producing pure brookite TiO_2 phase because it usually forms as a secondary minority phase along with the anatase or rutile phase and it has various physical properties [25,27–30]. A summary of the physical and structural properties of anatase and rutile phases of bulk TiO_2 has been given in Table 1.

In order to realize the vision of a clean society and our vision of plentiful research and innovation within the area that is rapidly expanding, the field of hydrogen economy is required. In the present study, the development of the TiO_2 nanotube arrays' phase structure under different heat treatment temperatures on the PEC water splitting hydrogen generation was investigated. Such a mechanistic understanding is very important for controlled growth of the suitable phase structure of TiO_2 nanotube arrays for high efficient PEC water splitting hydrogen generation.

2 Experimental

In the current study, self-organized TiO_2 nanotube arrays were prepared by anodization of high purity of Ti foils (99.6% purity with 0.127 mm in thickness) in a bath with electrolytes composed of ethylene glycol, ammonium fluoride (NH_4F) and hydrogen peroxide (H_2O_2). Anodization was done for 1 h at a constant potential of 60 V using a Keithley DC power supply. Based on our preliminary studies, H_2O_2 was maintained at 5 wt.% and continuous addition of small amount of H_2O_2 (≈ 0.5 mL) into the electrolyte at 5-min intervals was carried out because smooth and highly ordered TiO_2 nanotubes could be produced when they are maintained around this value [31,32]. The anodized Ti foils were cleaned using distilled water and dried under a nitrogen stream. The as-anodized samples were annealed in argon atmosphere, at 200–700 °C for 4 h.

The morphology of the anodized Ti foils was viewed via field emission scanning electron microscopy (FESEM, Zeiss SUPRA 35VP) at a working distance of approximately 1 mm and operating at 5 kV. The phase structure determination of TiO_2 nanotube arrays was determined by an X-ray diffraction (XRD) using Philips, PW 1729, operated at 45 kV and 40 mV. The PEC properties of the samples were characterized using a three-electrode PEC cell with TiO_2 nanotube arrays as the working photoelectrode, platinum rod as the counter electrode and saturated calomel electrode (SCE) as the reference electrode. A solution of 1 M KOH with 1 wt.% EG was used as the electrolyte. All three electrodes were connected to a potentiostat (μAutolab III). A 150 W xenon lamp (Zolix LSP-X150) with an intensity of 800 W/m^2 was used to produce a largely continuous and uniform spectrum; 100% of the light was transmitted by the quartz glass as the xenon lamp shone on the TiO_2 nanotube arrays (photoanode). The xenon lamp was switched on after the three electrodes were connected to the potentiostat. The H_2 evolution measurement was performed under a constant bias voltage of 0.6 V for 1 h and the evolved H_2 was collected using a reverted burette.

The corresponding photocurrent was measured during the voltage sweeping (5 mV/s). The photoconversion efficiency (η) of light to hydrogen energy was calculated based on the following equation:

$$\begin{aligned}\eta\,(\%) &= [(\text{total power output} - \text{electrical power output}) \\ &\quad /\text{light power input}] \times 100\% \\ &= j_\mathrm{p}\left[\left(E^\circ_\mathrm{rev} - |E_\mathrm{app}|\right)/I_\mathrm{o}\right] \times 100, \end{aligned} \quad (1)$$

where j_p is the photocurrent density (mA/cm^2); $j_\mathrm{p}E^\circ_\mathrm{rev}$ is the total power output; $j_\mathrm{p}|E_\mathrm{app}|$ is the electrical power input; I_o is the power density of the incident light (mW/cm^2); E°_rev is the standard reversible potential (1.23 V/SCE); $E_\mathrm{app} = E_\mathrm{mean} - E_\mathrm{aoc}$; E_mean is the electrode potential (versus SCE) of the working electrode, wherein the photocurrent is measured under illumination; and E_aoc is the potential (versus SCE) of the working electrode at open circuit condition.

3 Results and discussion

The as-anodized TiO_2 nanotubes were amorphous in nature [25,26]. Therefore, the main role of thermal treatment

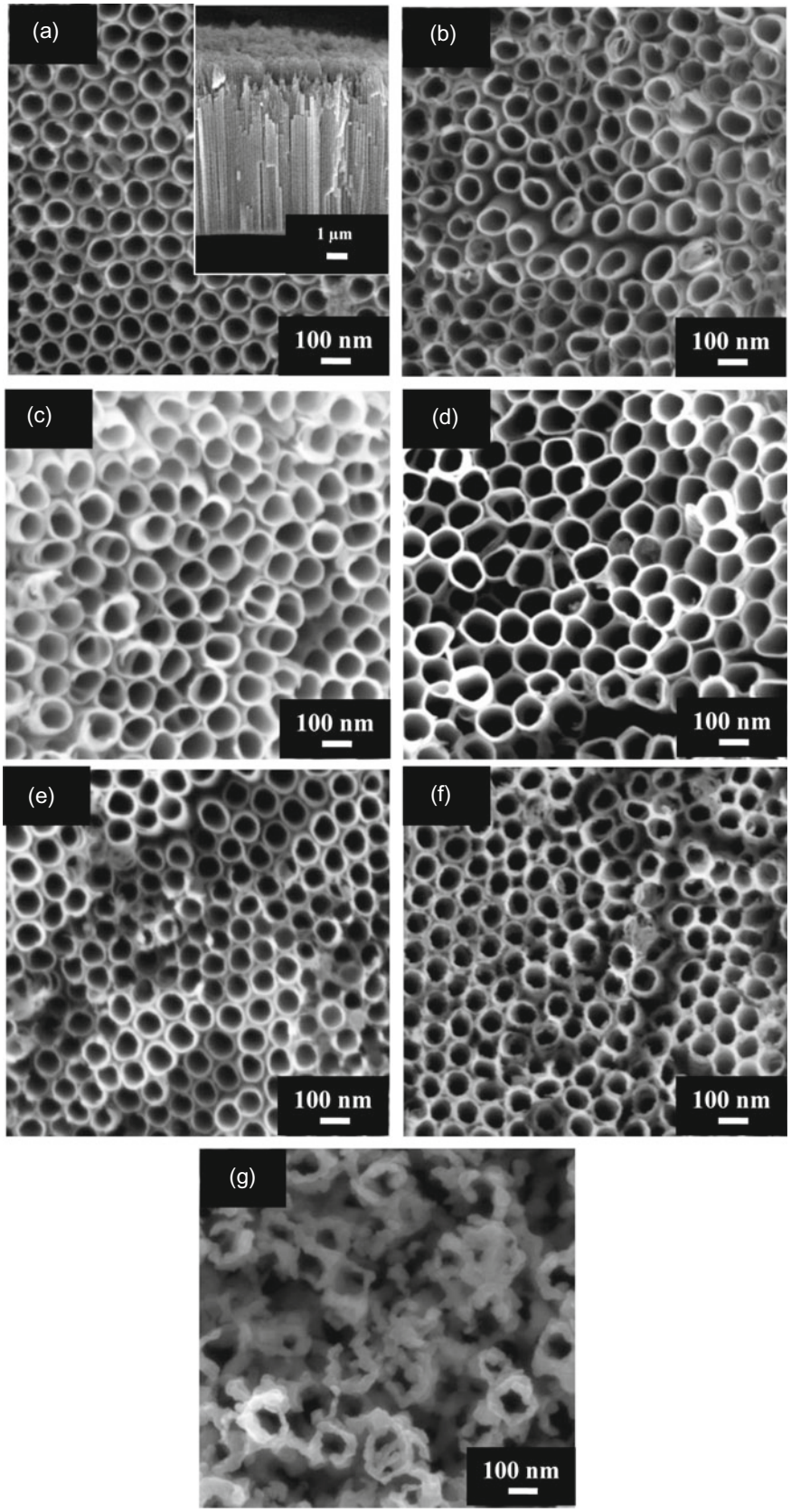

Fig. 1. FESEM micrographs of TiO_2 nanotube arrays annealed at different temperatures for 4 h in argon atmosphere, (a) as-anodized sample, (b) 200 °C, (c) 300 °C, (d) 400 °C, (e) 500 °C, (f) 600 °C and (g) 700 °C.

is to transform the amorphous phase to crystalline phase in a tube furnace [33,34]. In order to ensure the effect of thermal treatment on the morphology and phase transition of TiO_2 nanotube arrays, the samples were annealed from 200 °C to 700 °C. Figure 1 exhibits the FESEM images of the anodized TiO_2 nanotubes at different annealing temperatures. The heat treatment process has significant effects on the morphology of TiO_2 nanotubes. As shown in Figure 1a, as-anodized TiO_2 nanotubes with a diameter of 120 nm and a length of 12 μm were successfully produced. It was noticed that the nanotube structure would not be collapsed under the annealing temperature from 200 °C to 600 °C (Figs. 1b–1f). However, it is noteworthy to mention that the wall thickness of the nanotube was slightly increased as increasing the annealing temperatures. The wall thickness of nanotube was approximately 10 nm when annealed at 200 °C, while the wall thickness of the nanotube was raised to about 20 nm when annealed at 600 °C (Fig. 1e). The change in morphology of nanotube arrays with annealing temperature might be attributed to the excessive diffusion of Ti^{4+} ion along with the nanotube walls [25,35,36]. However, TiO_2 nanotube arrays were completely collapsed and destroyed at higher annealing temperature of 700 °C. These results were in agreement with the Grimes and coworkers' works in 2003 [37]. They proposed that nanotubes are stable up to 580 °C. The crystallization of the Ti substrate disturbed the tubular architecture causing collapse and sintering of the structure at higher annealing temperature. The reason for the collapse of the nanotubes was mainly attributed to the rutile protrusion emerging from the Ti structure at high temperature. Similar findings were reported by Schmuki's group [38] regarding the nanotube arrays that tend to suffer morphological deterioration at around 700 °C.

In this part of experiment, XRD analysis is used to investigate the effect of thermal treatment on the crystallization and phase transition of TiO_2 nanotube arrays. Figure 2 exhibits the XRD patterns of the TiO_2 nanotube arrays annealed at different temperatures. The result clearly shows that the crystal structure of TiO_2 is dependent on the thermal treatment. The XRD pattern of the as-anodized TiO_2 nanotube arrays exhibited Ti phase only, which indicates the amorphous nature of TiO_2 (Fig. 2a). The Bragg reflection of Ti phase was detected at 2θ values of 35.09°, 38.43°, 40.18°, 53.02°, 62.96°, 70.68°, 76.23° and 77.37° in all the XRD patterns, corresponding to (0 1 0), (0 0 2), (0 1 1), (0 1 2), (1 1 0), (0 1 3), (1 1 2) and (0 2 1) crystal planes, respectively. The presence of Ti phase was identified by the ICDD file of 44-1294. The XRD of the sample annealed at 200 and 300 °C indicates that the nanotubes have amorphous structure as only Ti peaks were observed (Figs. 2b and 2c). This indicates that annealing temperature was not sufficient to transform the amorphous phase into crystalline phase. Further increasing the annealing temperature to 400 °C has promoted the crystallization of anatase phase (Fig. 2d). This result indicates that TiO_2 is crystallized in anatase phase at a temperature between 350 °C and 400 °C. The obvious

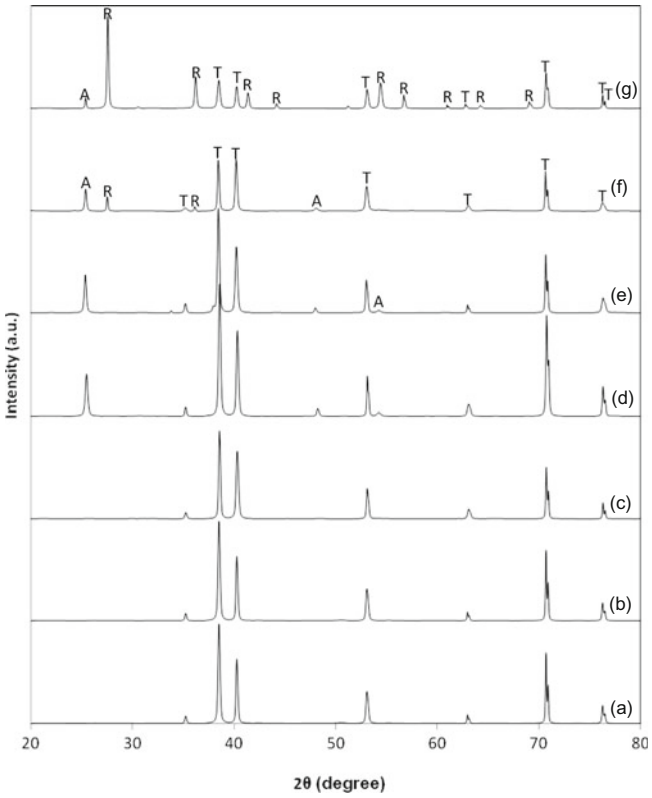

Fig. 2. XRD patterns of the TiO_2 nanotube arrays annealed at different temperatures, (a) as-anodized, (b) 200 °C, (c) 300 °C, (d) 400 °C, (e) 500 °C, (f) 600 °C and (g) 700 °C [A = anatase; T = titanium; R = rutile].

peaks were found at 25.37°, 48.21° and 54.10°, corresponding to (1 0 1), (2 0 0) and (1 0 5), crystal planes for the anatase TiO_2 nanotubes (ICDD No.: 21-1272). However, the anatase phase is still present dominantly at 500 °C and did not reveal any rutile phase in the XRD pattern as shown in Figure 2e. Further increasing the annealing temperature to 600 °C, the intensity of the anatase was decreasing and the existence of the rutile phase at 27.45° (1 1 0) and 36.07° (0 1 1) can be vaguely detected in the XRD pattern (Fig. 2f). Transformation of the anatase phase into rutile phase was observed after annealing at 600 °C. The anatase phase almost diminished and rutile as a major phase was observed at higher annealing temperature of 700 °C as exhibited in Figure 2g. The obvious rutile peaks were found at 27.45°, 36.07°, 41.24°, 44.08°, 54.34°, 56.67°, 62.72°, 64.10° and 69.04°, corresponding to (1 1 0), (0 1 1), (1 1 1), (1 2 0), (1 2 1), (2 2 0), (0 0 2), (1 3 0) and (0 3 1), respectively.

Subsequently, X-ray photoelectron spectroscopy (XPS) measurements were carried out to determine the surface chemical composition and oxidation state for certain samples annealed at different temperatures. The Ti XPS spectra are presented in Figure 3A. For as-anodized TiO_2 nanotubes, binding energy values of about 459.1 and 464.8 eV were detected, which matched with those of Ti $2p_{3/2}$ and Ti $2p_{1/2}$, respectively. It is noteworthy to point out that the binding energy of Ti $2p_{3/2}$ and Ti $2p_{1/2}$ was slightly

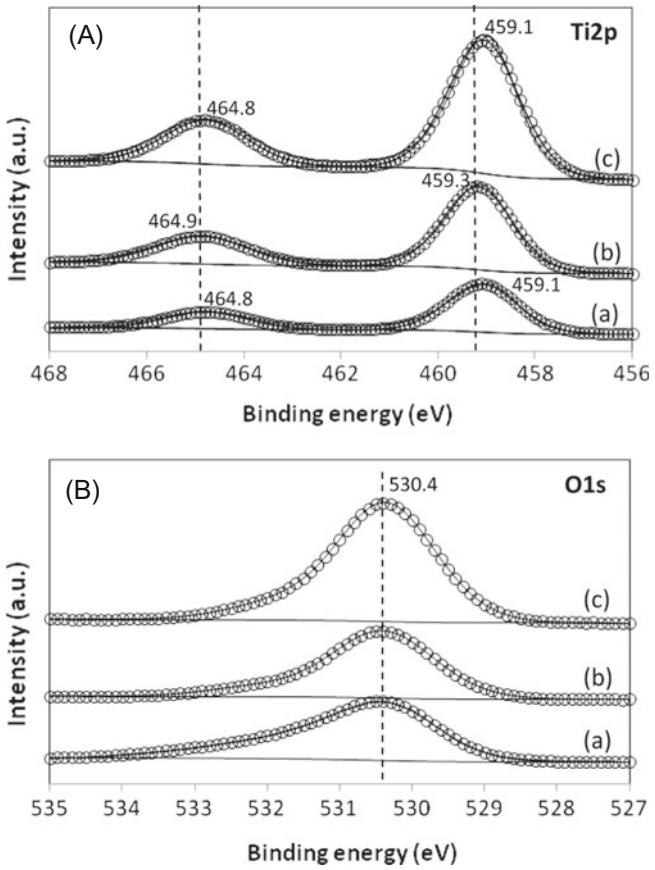

Fig. 3. XPS spectra of the (A) Ti 2p region and (B) O1 s region for (a) as-anodized sample, (b) sample annealed at 400 °C and (c) sample annealed at 600 °C.

positive shift to the 459.3 and 464.9 eV, respectively, for the sample annealed at 400 °C. The positive shift of the binding energy was mainly attributed to the oxygen vacancies decreased the electron cloud density associated with the Ti^{4+}. This statement was in good agreement with the earlier report of Mahajan et al., which suggested that reduction of oxygen vacancies caused a positive shift in binding energy [26]. However, the binding energy of Ti $2p_{3/2}$ and Ti $2p_{1/2}$ for the sample annealed at 600 °C was found similar to as-anodized TiO_2 nanotubes. This result infers the more oxygen-deficient structure within the polycrystalline sample than that of the single crystalline sample. In addition, polycrystalline sample might exhibited more surface defects, such as Ti^{3+} or oxygen vacancies, due to the lattice mismatch between anatase and rutile phase. Next, the binding energy values of the O1 s spectra are given in Figure 3B. The maximum peak at 530.4 eV was attributed to the lattice of oxygen. Interestingly, the full width at half-maximum of O1 s peaks were found broadened and the peaks' intensity was increased for the as-anodized sample and sample annealed at 600 °C. The reason might be related to the presence of higher oxygen vacancies' concentration within the lattice.

Previous studies have indicated that as-anodized nanotubes develop as an amorphous structure [25,34,39]. It is of interest to establish how the anodic TiO_2 nanotube arrays change following a heat treatment process, which is required to convert the as-prepared amorphous structure into a fully crystalline structure of nanotube arrays. Therefore, comprehensive work on the PEC water splitting hydrogen generation by using the above-discussed samples as photoelectrode in PEC cell has been investigated. The experimental conditions for the selected samples with different crystal structure are summarized in Table 2.

Table 2. Experimental conditions used to achieve different crystal structure of nanotube arrays, which is synthesized in ethylene glycol electrolyte containing 5 wt.% H_2O_2 and 5 wt.% NH_4F for 1 h at 60 V.

Sample	Annealing temperature	Crystal structure	Morphology
A	As-anodized sample	Amorphous	Nanotubes
B	300 °C, 4 h, argon	Amorphous	Nanotubes
C	400 °C, 4 h, argon	Anatase	Nanotubes
D	500 °C, 4 h, argon	Anatase	Nanotubes
E	600 °C, 4 h, argon	Anatase + rutile	Nanotubes
F	700 °C, 4 h, argon	Anatase + rutile	Nanoporous

Based on the results of *I-V* characteristic curves (Fig. 4), amorphous TiO_2 nanotubes (sample A) showed poor photocurrent density among the samples of ≈ 0.03 mA/cm^2. The reason might be attributed to the presence of oxygen vacancies within the bulk, which increases the number of recombination centers significantly. These recombination centers obviously decrease the mobility of photo-induced electrons due to the increased series of resistance caused by these trap states. As a consequence, positive holes acted as electron acceptor states on the nanotube surface and hindered the transportation of photo-induced electrons from the nanotube surface to the Ti substrate for photocurrent generation. Besides, amorphous phase comprises of various defects such as impurities, dangling bonds and micro-voids, which could also be acting as recombination centers and result in a decrease of photocurrent density. Most importantly, an amorphous TiO_2 nanotube is basically unable to develop a regular depletion region (space charge layer), where transportation of charge carriers takes place [40]. This suggests that improved crystallinity of the samples can effectively increase the photocurrent density due to the development of a depletion layer and reduction in recombination centers [17,19,40].

The photocurrent density was found to increase for annealed samples. However, the photocurrent density of sample B slightly increased to 0.15 mA/cm^2. The reason might be attributed to the annealing temperature of 300 °C which was not sufficient to transform the amorphous phase into crystalline phase as explained previously. Therefore, it showed the poor photocurrent density as seen in Figure 4e. Sample C annealed at 400 °C showed the highest photocurrent density throughout the potential window, suggesting that an efficient charge separation occurred and the photocurrent reached a high value

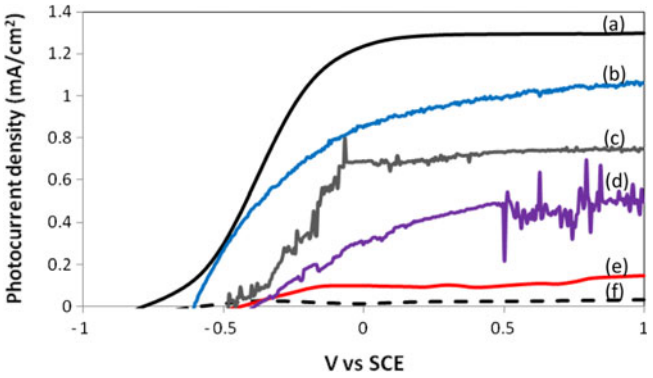

Fig. 4. (Color online) *I-V* characteristics of TiO_2 nanotube arrays with different crystal structure, (a) sample C, (b) sample D, (c) sample E, (d) sample F, (e) sample B and (f) sample A.

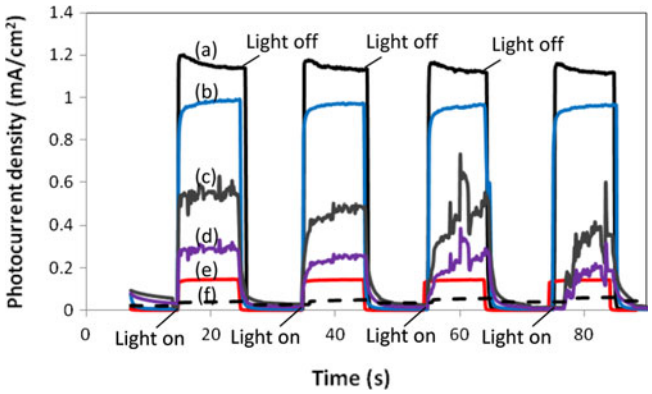

Fig. 5. (Color online) Potentiostatic plot of TiO_2 nanotube arrays with different crystal structure, (a) sample C, (b) sample D, (c) sample E, (d) sample F, (e) sample B and (f) sample A.

of 1.25 mA/cm^2 (Fig. 4a). The increase in photocurrent density is likely attributed to the higher photo-induced electron/hole pairs caused by the highly single crystalline of anatase phase [26]. Sample D showed a slightly decreasing photocurrent density to 1 mA/cm^2 compared to sample C (Fig. 4b). The reason may be attributed to the phase transformation from anatase phase to rutile phase which was started during the heat treatment process. It is noteworthy to mention that the photocurrent density curve starts showing the fluctuation line, which indicated that the mobility of the photo-induced electrons was affected. The reason probably is due to the scattering problem of photo-induced electrons within the lattice of polycrystalline structure [25,26,35]. In fact, single crystal structure has periodic arrangement of the atoms (anatase), whereas polycrystalline structure shows periodic arrangement of atoms in different regions (anatase and rutile) [27]. This statement is further confirmed with the results exhibited by the samples E and F (polycrystalline nature of anatase and rutile phases). As seen from Figures 4c and 4d, samples E and F exhibited extreme fluctuation photocurrent density curve with 0.7 mA/cm^2 and 0.5 mA/cm^2, respectively. The reason might be related to the collapsed nanotube structure at higher annealing temperature, which may create difficult diffusion path for photo-induced electrons and eventually decreased the cell photocurrent. In addition, difference in specific surface area and crystal size between the anatase and rutile phase may also cause defect sites trapping sites and disordered contact areas between the TiO_2 atoms as summarized in Table 1 [26,27]. Therefore, the transportation time and distance of photo-induced electrons are longer, which results in more charge carriers' recombination and enhanced scattering of free electrons [24,41]. As a result, critical fluctuation photocurrent density curves were observed and exhibited poor photocurrent performances. This is in agreement with the results of Sclafani and Herrnann's work [42] and Jaturong's work [43], which proposed that anatase TiO_2 phase is more photoactive than the rutile phase due to its larger specific surface area and easy hydroxylation.

The above-discussed statement is further confirmed by open-circuit photovoltage (Voc), which is the maximum photovoltage that can be obtained from the PEC cell when its terminals are left open. As shown in Figure 4, a more negative value of photovoltage for sample C (−0.8 V) followed by sample A (−0.65 V), sample D (−0.65 V), sample E (−0.5 V), sample F (−0.45 V) and sample B (−0.45 V), is obtained. These more negative Voc values indicate that the lifetime of the charge carriers was increased and the recombination rate of charge carriers was reduced. These results were almost in line with the photocurrent density generation. However, Voc for cell built with sample A (amorphous) was higher than those built with samples E and F (polycrystalline). The reason was mainly attributed to the higher concentration of oxygen vacancies on the amorphous TiO_2 surface, which led to an increase in the dissociative adsorption rate of water and increased density of hydroxyl radicals (OH) adsorbed on the TiO_2 surface. Liu et al. have claimed that these OH act as a potential barrier in the solid/liquid interface, thus, avoiding the back reaction. As a consequence, a higher Voc value was achieved for the amorphous (sample A) [44].

Next, the responsiveness of the TiO_2 nanotube arrays with different crystal structure toward the interruption of light was studied at a fixed bias voltage of 0.6 V vs. SCE. The potentiostatic plots of the photocurrent density are measured and exhibited in Figure 5. Good photoresponses were recorded for the sample A, sample B, sample C and sample D under light on-off conditions. As shown in Figure 5, the photocurrent pattern was highly reproducible for numerous on-off-cycles. However, sample E and sample F (polycrystalline of anatase and rutile TiO_2) exhibited the fluctuation photocurrent as shown in Figures 5c and 5d. As explained previously, the current fluctuations in polycrystalline TiO_2 nanotube arrays are probably due to the defect sites and trapping sites for photo-induced electrons within the bulk of TiO_2 nanotubes, which act as recombination centers for photo-induced charge carriers.

To estimate the quantitative correlation of light absorption to the different crystal structure of TiO_2 nanotubes, the photoconversion efficiency (η) of light to hydrogen energy was measured (Fig. 6). The highest photoconversion efficiency of about 3.1% was obtained for sample C annealed at 400 °C. The decrease in

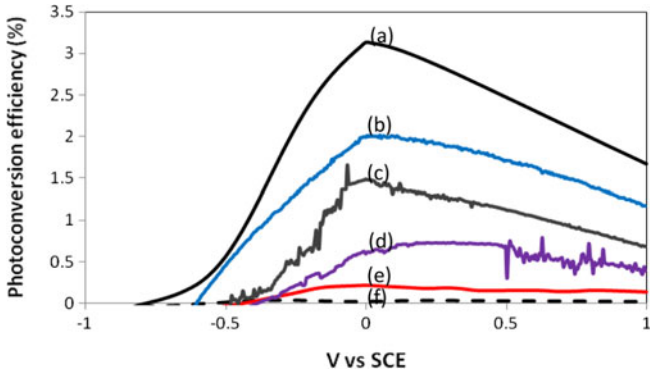

Fig. 6. (Color online) Photoconversion efficiency of TiO_2 nanotube arrays with different crystal structure, (a) sample C, (b) sample D, (c) sample E, (d) sample F, (e) sample B and (f) sample A.

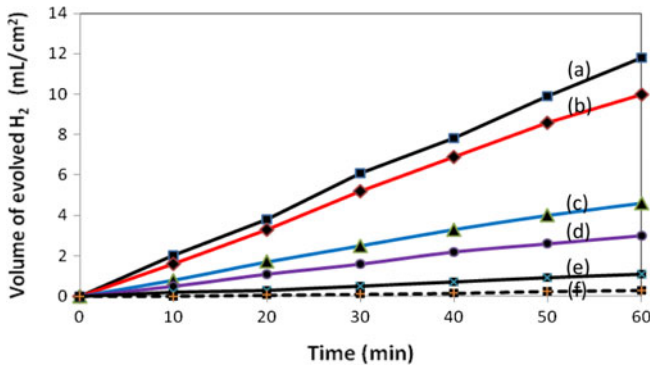

Fig. 7. (Color online) H_2 evolution TiO_2 nanotube arrays with different crystal structure, (a) sample C, (b) sample D, (c) sample E, (d) sample F, (e) sample B, and (f) sample A.

photocurrent efficiency was as follows, 2.0%, 1.5%, 0.8%, 0.2% and 0.05% corresponding to sample D, sample E, sample F, sample B and sample A. The results show that there is a distinct dependency of the PEC properties on the crystal structure of TiO_2 nanotube arrays. In this aspect, the 400 °C-annealed TiO_2 nanotube arrays (sample C) exhibited the best PEC response.

Figure 7 shows the relation between the total hydrogen volume and the operation time. A maximum evolution rate of the hydrogen of 190 μL/cm^2/min was achieved from the photoelectrode (sample C), which has higher crystallinity of anatase phase. This result indicates that high crystallinity with anatase phase is favorable for hydrogen production. The decrease in the rate of hydrogen production was as follows: 165 μL/cm^2/min, 75 μL/cm^2/min, 55 μL/cm^2/min, 15 μL/cm^2/min and 5 μL/cm^2/min, which correspond to the sample D, sample E, sample F, sample B and sample A, respectively.

4 Conclusion

The present study demonstrated that the role of heat treatment process is to transform the amorphous structure of TiO_2 nanotube arrays into the crystalline phase. The as-anodized TiO_2 nanotube arrays were amorphous in nature. It was found that the TiO_2 nanotube arrays were crystallized in highly anatase phase at temperature 400 °C and transformation of anatase to rutile phase was observed at temperature 600 °C. However, TiO_2 nanotube arrays were completely collapsed at higher annealing temperature of 700 °C because of the rutile protrusion emerging from the Ti structure at higher temperature. TiO_2 nanotube arrays annealed at 400 °C showed the highest photocurrent density throughout the potential window, suggesting that an efficient charge separation occurred and the photocurrent reached a high value of 1.25 mA/cm^2 with 3.1% of photoconversion efficiency. The evolution rate of the hydrogen gas of 190 μL/cm^2/min was achieved from the reverted burette. The main reason might be attributed to the single crystalline of anatase phase with periodic arrangement of atoms which provides a better transportation pathway to the photo-induced electrons compared to the amorphous and polycrystalline anatase and rutile phases within the TiO_2 nanotube arrays. Therefore, it has been acknowledged as the most efficient form for the PEC water splitting hydrogen generation.

The author would like to thank Universiti Sains Malaysia for sponsoring this work under RU Grant No. 814075, RU Grant No. 814154, PRGS Grant No. 8044058, FRGS Grant No. 6071213, Fellowship USM and Research University Postgraduate Research Grant Scheme, 80430146.

References

1. J.A. Turner, Science **285**, 687 (1999)
2. M. Jefferson, Renew. Energy **31**, 571 (2006)
3. T.K. Tromp, R.L. Shia, M. Allen, J.M. Eiler, Y.L. Yung, Science **300**, 1740 (2003)
4. V.M. Aroutiounian, V.M. Arakelyan, G.E. Shahnazaryan, Sol. Energy **78**, 581 (2005)
5. E.Y. Kim, J.H. Park, G.Y. Han, J. Power Sources **184**, 284 (2008)
6. W. Kreuter, H. Hofmann, Int. J. Hydrogen Energy **23**, 661 (1998)
7. V.K. Mahajan, S.K. Mohapatra, M. Misra, Int. J. Hydrogen Energy **33**, 5369 (2008)
8. S.K. Mohapatra, M. Misra, V.K. Mahajan, K.S. Raja, J. Catal. **246**, 362 (2007)
9. M. Paulose, G.K. Mor, O.K. Varghese, K. Shankar, C.A. Grimes, J. Photoch. Photobio. A **178**, 8 (2006)
10. P.R. Mishra, P.K. Shukla, A.K. Singh, O.N. Srivastave, Int. J. Hydrogen Energy **28**, 1089 (2003)
11. Z. Zhang, M.F. Hossain, T. Takahashi, Int. J. Hydrogen Energy **35**, 8528 (2010)
12. G.K. Mor, K. Shankar, O.K. Varghese, C.A. Grimes, Nano Lett. **19**, 2989 (2004)
13. A. Fujishima, K. Honda, Nature **238**, 37 (1972)
14. M. Grätzel, Nature **414**, 338 (2001)
15. C.W. Lai, S. Sreekantan, J. Nanomater. **2011**, 142463 (2011)
16. P. Roy, S. Berger, P. Schmuki, Angew. Chem. Int. Ed. **50**, 2904 (2011)

17. L.D. Sun, S. Zhang, X.W. Sun, X.D. He, J. Nanosci. Nanotechnol. **10**, 4551 (2010)
18. C.W. Lai, S. Sreekantan, Z. Lockman, J. Nanosci. Nanotechnol. **12**, 4057 (2012)
19. C.W. Lai, S. Sreekantan, Int. J. Photoenergy **2012**, 356943 (2012)
20. M. Ni, M.K.H. Leung, D.Y.C. Leung, K. Sumathy, Renew. Sust. Energ. Rev. **11**, 401 (2007)
21. N.K. Allam, K. Shankar, C.A. Grimes, J. Mater. Chem. **18**, 2341 (2008)
22. C.A. Grimes, J. Mater. Chem. **17**, 1451 (2007)
23. D. Wang, Y. Liu, B. Yu, F. Zhou, W. Liu, Chem. Mater. **21**, 1198 (2009)
24. J.F. Yan, F. Zhou, J. Mater. Chem. **21**, 9406 (2011)
25. G.K. Mor, O.K. Varghese, M. Paulose, K. Shankar, C.A. Grimes, Sol. Energy Mater. Sol. Cells **90**, 2011 (2006)
26. V.K. Mahajan, M. Misra, K.S. Raja, S.K. Mohapatra, J. Phys. D.: Appl. Phys. **41**, 125307 (2008)
27. A. Fujishima, X.T. Zhang, D.A. Tryk, Surf. Sci. Rep. **63**, 515 (2008)
28. M. Addamo, M. Bellardita, A.D. Paola, L. Palmisano, Chem. Commun. **47**, 4943 (2006)
29. H. Zhang, J.F. Banfield, J. Phys. Chem. B **104**, 3481 (2000)
30. R. Hengerer, B. Bolliger, M. Erbudak, M. Gratzel, Surf. Sci. **460**, 162 (2000)
31. S. Sreekantan, C.W. Lai, Z. Lockman, J. Electrochem. Soc. **158**, 397 (2011)
32. C.W. Lai, S. Sreekantan, Micro Nano Lett. **7**, 443 (2012)
33. C.W. Lai, S. Sreekantan, P.S. E, J. Mater. Res. **27**, 1695 (2012)
34. D. Regonini, A. Jaroenworaluck, R. Stevens, C.R. Bowen, Surf. Interface Anal. **42**, 139 (2010)
35. Y.K. Lai, J.Y. Huang, H.F. Zhang, V.P. Subramaniam, Y.X. Tang, D.G. Gong, L. Sundar, L. Sun, Z. Chen, C.J. Lin, J. Hazard. Mater. **184**, 855 (2010)
36. S. Sreekantan, R. Hazan, Z. Lockman, Thin Solid Films **518**, 16 (2009)
37. O.K. Varghese, D. Gong, M. Paulose, C.A. Grimes, E.C. Dickey, J. Mater. Res. **18**, 156 (2003)
38. A. Ghicov, P. Schmuki, Chem. Commum. **20**, 2791 (2009)
39. R. Mohammadpour, A. Iraji Zad, M.M. Ahadian, N.N. Taghavinia, A. Dolati, Eur. Phys. J. Appl. Phys. **47**, 10601 (2009)
40. K.S. Ahn, S.H. Lee, A.C. Dillon, E. Tracy, R. Pitts, J. Appl. Phys. **101**, 093524 (2007)
41. Y. Inoue, Enery Environ. Sci. **2**, 364 (2009)
42. A. Sclafani, J.M. Hermann, J. Photochem. Photobiol. A **113**, 181 (1998)
43. J. Jaturong, P. Sarapong, S. Yoshikazu, Y. Susumu, J. Solid State Chem. **180**, 1743 (2007)
44. Y. Liu, A. Hagfeldt, X.R. Xiao, S.E. Lindquist, Sol. Energy Mater. Sol. Cells **55,** 267 (1998)